NATIONAL ADVISORY COMMITTEE FOR AERONAUTICS

TECHNICAL NOTE 2698

THEORETICAL ANALYSIS OF HYDRODYNAMIC IMPACT OF A PRISMATIC FLOAT HAVING FREEDOM IN TRIM

By Robert W. Miller

Langley Aeronautical Laboratory
Langley Field, Va.

Washington

June 1952

1W

NATIONAL ADVISORY COMMITTEE FOR AERONAUTICS

TECHNICAL NOTE 2698

THEORETICAL ANALYSIS OF HYDRODYNAMIC IMPACT OF A PRISMATIC FLOAT HAVING FREEDOM IN TRIM

By Robert W. Miller

SUMMARY

Equations which include freedom in trim are derived for hydrodynamic impact of a non-chine-immersed, prismatic float forebody having a V-bottom and a transverse step. These equations are an extension of previously published fixed-trim theory, and a method of solution is indicated by which time histories of vertical, horizontal, and angular displacement, velocity, and acceleration can be obtained.

Comparisons of specific solutions of the equations with corresponding fixed-trim solutions are presented. The trends and deviations noted are similar to those exhibited by a like comparison of experimental data for free- and fixed-trim impacts.

INTRODUCTION

Previously published hydrodynamic impact theory (references 1 to 3) has been based on the concept that the flow about an immersing seaplane float or hull is a two-dimensional phenomenon occurring in transverse planes fixed in space and oriented normal to the keel. The total force on the float is obtained by summing the reactions in the individual flow planes in contact with the float and applying an aspect-ratio correction factor to account for the end-flow losses which exist in three-dimensional flow. This theory has made use of the simplifying assumption that the trim remains fixed throughout the impact. Experimental checks of this fixed-trim theory for both model and full-scale hulls have been presented in numerous reports and some evaluation of the empirical factors involved has been conducted.

The present investigation was initiated in order to obtain a method for determining the effect of freedom in trim on loads, moments, and motions during hydrodynamic impacts of a non-chine-immersed, prismatic float forebody having a V-bottom and a transverse step. As in the previous theoretical presentations the wing lift was assumed to be equal to the model weight and the aerodynamic moments were neglected in order

to simplify the problem, although they might have had an appreciable stabilizing effect.

The present paper is primarily concerned with the derivation of equations describing the vertical, longitudinal, and angular motions and accelerations of the previously described float during hydrodynamic impact. It also presents comparisons of numerical solutions of these equations with theoretical fixed-trim loads, moments, and motions under identical initial conditions, and a comparison is made of experimental free-trim and fixed-trim data.

SYMBOLS

A	hydrodynamic aspect ratio $(\tan \beta/\tan \tau)$
a	distance between center of gravity and step, parallel to keel
b	distance between center of gravity and step, normal to keel
F	hydrodynamic force
I_{cg}	moment of inertia about center of gravity (pivot point)
K	constant $\left(\frac{1}{2}\rho\pi F(\beta)\right)$
l	wetted keel length
M_{cg}	moment about center of gravity (bow-up moment is positive)
M_s	moment about step
m_f	virtual mass of float
m_w	mass of fluid in a flow plane
$\ddot{S}$	acceleration of center of gravity, parallel to keel
s	distance of flow plane forward of step, parallel to keel
t	time after contact
V	velocity
$\ddot{X}$	horizontal acceleration of center of gravity

x	horizontal displacement of step from contact point
$\ddot{Y}$	vertical acceleration of center of gravity
y	draft at step
$\ddot{Z}$	acceleration of center of gravity, normal to keel
z	penetration of float into a flow plane
β	angle of dead rise
γ	flight-path angle $\left(\tan^{-1}\frac{\dot{y}}{\dot{x}}\right)$
ρ	mass density of water
τ	trim, radians, except as noted
$F(\beta)$	dead-rise function
$\varphi(A)$	aspect-ratio correction factor

Subscripts:

o	condition at time of water contact
n	direction normal to keel
p	direction parallel to keel

Where units are not specified any consistent system of units may be used.

Dots over x, y, z, and τ indicate differentiation with respect to time.

METHOD OF ANALYSIS

Physical concepts.- The physical concepts on which this analysis is based are discussed in detail in references 1 and 3, in which the solution is restricted to fixed positive trim. Briefly, the theory discussed in these references was based on the concept that the primary flow about an immersing seaplane float or hull occurs in transverse planes which were considered fixed in space and oriented perpendicular to the keel. Figure 1 is a sketch of a prismatic float immersing at positive trim.

A given flow plane is indicated in figure 1(a) at a distance s forward of the step and the penetration of the float into this flow plane is represented by z. The motion of the fluid in each plane was treated as a two-dimensional phenomenon independent of the other flow planes.

The total force on the float is obtained by integrating the reactions of the fluid in the individual flow planes in contact with the float. This force is reduced by the application of an end-flow (aspect-ratio) correction to account for the losses which exist in three-dimensional flow. The effects of buoyancy and viscosity are neglected, since in an impact they are normally small in comparison with the inertia forces. A lift force equal to the weight of the seaplane is also assumed to act throughout the impact.

These concepts are followed in the present analysis except for the modifications necessary to introduce freedom in trim. In order to introduce freedom in trim, the flow planes are assumed to rotate about instantaneous centers of rotation at their intersection with the float keel. Thus, the planes are permitted to maintain their orientation normal to the keel and at the same time to have no translation in space along the line of the keel.

Equations of motion.- In this analysis both the float being considered and the forces applied to it are symmetrical about a vertical plane through the keel so that the float motions can be resolved as a case of plane motion. The equations of motion for the float (see fig. 1(a)) can then be written as

$$F_p = -m_f\ddot{S} \tag{1}$$

$$F_n = -m_f\ddot{Z} \tag{2}$$

$$M_{cg} = I_{cg}\ddot{\tau} \tag{3}$$

In equations (1) and (2) the quantities $\ddot{S}$ and $\ddot{Z}$ are the components of the center-of-gravity acceleration which are, respectively, parallel and perpendicular to the keel. These accelerations can be expressed in terms of the horizontal and vertical components of the step acceleration and the center-of-gravity accelerations relative to the step in the following manner:

$$\ddot{S} = \ddot{x}\cos\tau - \ddot{y}\sin\tau - a\dot{\tau}^2 - b\ddot{\tau} \tag{4}$$

and

$$\ddot{Z} = \ddot{y} \cos \tau + \ddot{x} \sin \tau + b\dot{\tau}^2 - a\ddot{\tau} \tag{5}$$

Since the viscous forces of the fluid are considered small enough to be neglected in this analysis, there is no force on the float in the direction parallel to the keel and hence F_p is equal to zero. Therefore, from equations (1) and (4) the following expression can be obtained:

$$0 = -m_f(\ddot{x} \cos \tau - \ddot{y} \sin \tau - a\dot{\tau}^2 - b\ddot{\tau}) \tag{6}$$

This equation can then be solved to obtain an expression for $\ddot{x}$:

$$\ddot{x} = \frac{\ddot{y} \sin \tau}{\cos \tau} + \frac{a\dot{\tau}^2}{\cos \tau} + \frac{b\ddot{\tau}}{\cos \tau} \tag{7}$$

Now consider equation (2), the normal-force equation. The normal force on the float is the sum of the forces exerted by the individual flow planes reduced by an end-flow-loss correction factor. The typical flow plane illustrated in figure 1(a) is at a distance s forward of the step and has a width ds parallel to the keel. The float has made a penetration z into the plane. From the analysis of reference 3, the virtual mass of fluid in this flow plane is

$$m_w = Kz^2 ds \tag{8}$$

where

$$K = \frac{1}{2}\rho\pi F(\beta) \tag{9}$$

In accordance with the assumptions, the reaction of the fluid in the plane is the time derivative of the momentum so that

$$dF = \frac{d}{dt}(m_w\dot{z}) = \frac{d}{dt}(Kz^2 ds\ \dot{z}) = K(z^2\ddot{z} + 2z\dot{z}^2)ds \tag{10}$$

The normal force acting on the float can now be obtained by integrating over the wetted length and multiplying by the aspect-ratio correction factor

$$F_n = \varphi(A) \int_0^{s=l} dF = K\varphi(A) \int_0^{y/\sin\tau} (z^2\ddot{z} + 2z\dot{z}^2)ds \tag{11}$$

where F_n can be seen to be a function of z, $\dot{z}$, and $\ddot{z}$. These quantities may be established as follows.

It can be seen from figure 1(a) that the penetration z of the float into a given flow plane can be written as a function of the variables y, s, and τ, each of which is a function of time. Thus

$$z = \frac{y}{\cos\tau} - \frac{s\sin\tau}{\cos\tau} \tag{12}$$

Differentiation of z with respect to time gives

$$\dot{z} = \frac{\dot{y}}{\cos\tau} - \frac{\dot{s}\sin\tau}{\cos\tau} + \frac{y\dot{\tau}\sin\tau}{\cos^2\tau} - \frac{s\dot{\tau}}{\cos^2\tau} \tag{13}$$

and a further differentiation gives

$$\ddot{z} = \frac{\ddot{y}}{\cos\tau} - \frac{\ddot{s}\sin\tau}{\cos\tau} + \frac{y\ddot{\tau}\sin\tau}{\cos^2\tau} - \frac{s\ddot{\tau}}{\cos^2\tau} + \frac{y\dot{\tau}^2}{\cos\tau} + \frac{2y\dot{\tau}^2\sin^2\tau}{\cos^3\tau} - \frac{2s\dot{\tau}^2\sin\tau}{\cos^3\tau} + \frac{2y\dot{\tau}^2\sin\tau}{\cos^2\tau} - \frac{2\dot{s}\dot{\tau}}{\cos^2\tau} \tag{14}$$

The derivatives $\dot{s}$ and $\ddot{s}$ are now expressed in terms of x, y, and τ. In accordance with the assumptions, the velocity $\dot{s}$ is constant over the wetted length and is simply equal to the negative of the float tangential velocity V_p; thus, from figure 1(b),

$$\dot{s} = -V_p = \dot{y} \sin \tau - \dot{x} \cos \tau \tag{15}$$

The derivative of this expression is

$$\ddot{s} = \frac{d\dot{s}}{dt} = \ddot{y} \sin \tau - \ddot{x} \cos \tau + \dot{y}\dot{\tau} \cos \tau + \dot{x}\dot{\tau} \sin \tau$$

Introducing equation (7) gives

$$\ddot{s} = \dot{y}\dot{\tau} \cos \tau + \dot{x}\dot{\tau} \sin \tau - a\dot{\tau}^2 - b\ddot{\tau} \tag{16}$$

Equations (12), (13), and (14), with $\dot{s}$ and $\ddot{s}$ replaced by equations (15) and (16), respectively, are now introduced into equation (11). Integration is then performed to obtain the normal force in terms of motions of the step. Substituting the resulting expression for normal force into equation (2), where $\ddot{Z}$ in this equation is replaced by equation (5), gives the following equation for motion of the center of gravity normal to the keel:

$$\frac{K\varphi(A)}{12 \sin^3\tau \cos^5\tau}\left\{y^4\left[\ddot{\tau}(4 \sin^3\tau \cos \tau - \sin \tau \cos \tau) + \dot{\tau}^2(16 \sin^4\tau - 6 \sin^2\tau + 2)\right] + y^3\left[\ddot{y}(4 \sin^2\tau \cos^2\tau) + \ddot{\tau}(4b \sin^3\tau \cos^2\tau) + \dot{\tau}^2(4a \sin^3\tau \cos^2\tau) + \dot{x}\ddot{\tau}(20 \sin^4\tau \cos^2\tau) + \dot{y}\dot{\tau}(12 \sin \tau \cos^3\tau - 20 \sin \tau \cos^5\tau)\right] + y^2\left[12 \sin^2\tau \cos^4\tau(\dot{y} \cos \tau + \dot{x} \sin \tau)^2\right]\right\} =$$

$$-m_f\left(\frac{\ddot{y}}{\cos \tau} + \frac{b\ddot{\tau} \sin \tau}{\cos \tau} + b\dot{\tau}^2 - a\ddot{\tau} + \frac{a\dot{\tau}^2 \sin \tau}{\cos \tau}\right) \tag{17}$$

In order to solve the third equation of motion, the total moment exerted by the individual flow planes about the center of gravity must be determined. To make an approximate correction for end-flow losses this moment is multiplied by the aspect-ratio factor $\varphi(A)$, where the assumption is made that this over-all correction factor can be applied to the moment as well as to the normal force. Equation (3) may thus be written as

$$M_{cg} = \varphi(A) \int (s - a)dF = I_{cg}\ddot{\tau} \tag{18}$$

which, with the use of equation (11), becomes

$$M_{cg} = K\varphi(A) \int_0^{y/\sin \tau} (z^2\ddot{z} + 2z\dot{z}^2)s \, ds - aF_n \tag{19}$$

Proceeding as with the normal-force equation gives the following equation for angular motion about the center of gravity:

$$\frac{K\varphi(A)}{60 \sin^4\tau \cos^5\tau}\left\{y^5\left[\ddot{\tau}(5 \sin^3\tau \cos \tau - 2 \sin \tau \cos \tau) + \dot{\tau}^2(25 \sin^4\tau - 19 \sin^2\tau + 6)\right] + y^4\left[\ddot{y}(5 \sin^2\tau \cos^2\tau) + \ddot{\tau}(5a \sin^2\tau \cos \tau - 20a \sin^4\tau \cos \tau + 5b \sin^3\tau \cos^2\tau) + \dot{\tau}^2(35a \sin^3\tau - 85a \sin^5\tau - 10a \sin \tau) + \dot{x}\dot{\tau}(25 \sin^2\tau \cos^2\tau - 35 \sin^2\tau \cos^4\tau) + \dot{y}\dot{\tau}(15 \sin \tau \cos^3\tau - 35 \sin \tau \cos^5\tau)\right] + y^3\left[-\ddot{y}(20a \sin^3\tau \cos^2\tau) - \ddot{\tau}(20ab \sin^4\tau \cos^2\tau) - \dot{\tau}^2(20a^2 \sin^4\tau \cos^2\tau) - \dot{x}\dot{\tau}(100a \sin^5\tau \cos^2\tau) + \dot{y}\dot{\tau}(40a \sin^2\tau \cos^3\tau - 100a \sin^4\tau \cos^3\tau) + 20 \sin^2\tau \cos^4\tau(\dot{y} \cos \tau + \dot{x} \sin \tau)^2\right] - y^2\left[60a \sin^3\tau \cos^4\tau(\dot{y} \cos \tau + \dot{x} \sin \tau)^2\right]\right\} = I_{cg}\ddot{\tau} \tag{20}$$

Equations (7), (17), and (20) are the equations of motion for the float and involve the three unknowns x, y, and τ. These equations can be solved numerically for the time histories of the three variables and their derivatives; see appendix A for a step-by-step iteration process. Involved in the solution of these equations are the dead-rise function (see equation (9)) and the aspect-ratio correction factor (see equation (11)), which are discussed in the subsequent section.

Factors $F(\beta)$ and $\varphi(A)$.- In order to perform the numerical solutions expressions must be obtained for the dead-rise function $F(\beta)$ and the aspect-ratio correction factor $\varphi(A)$ contained in the normal-force and moment equations.

An expression for the dead-rise function $F(\beta)$, which gives the variation of the effective two-dimensional fluid mass with dead rise, was given by Wagner in reference 4 as

$$F(\beta) = \left(\frac{\pi}{2\beta} - 1\right)^2$$

which is equivalent to $\left[f(\beta)\right]^2$ of reference 3.

Although this relationship has not been experimentally verified for impacts of floats having low dead-rise angles, it has been found to be in substantial agreement with test data obtained with floats of $22\frac{1}{2}^\circ$ to 40° angle of dead rise (see reference 3).

On the basis of experiments with vibrating plates in water (reference 5), Pabst derived the following aspect-ratio expression for approximating the three-dimensional virtual mass from the virtual mass computed on a two-dimensional basis:

$$\varphi(A) = 1 - \frac{1}{2A}$$

where A is the aspect ratio of the equivalent vibrating plate. If this reduction in the virtual mass is assumed to be determined by the shape of the intersected area in the plane of the water surface, then the application of Pabst's data to V-bottom floats results in the expression

$$\varphi(A) = 1 - \frac{\tan \tau}{2 \tan \beta}$$

THEORETICAL RESULTS

Reduction to fixed trim.- The free-trim equations were derived from the same basic assumptions as the fixed-trim equations; they must, therefore, be reducible to the fixed-trim equations. This reduction is accomplished in appendix B by considering the trim to be a constant instead of a variable, so that the terms containing $\dot{\tau}$ and $\ddot{\tau}$ drop out. It is then demonstrated that equations (17) and (20) reduce to a form identical with the equations for normal force and step moment in references 1 and 6, respectively. Equation (7) is also shown to reduce to a simple fixed-trim relation.

Comparison of free- and fixed-trim theoretical solutions.- In order to indicate the effect of freedom in trim both free- and fixed-trim theoretical solutions were made for a typical hull for three different sets of landing conditions. The dimensions and inertia values of the full-scale float considered are given in table I. The theoretical initial conditions for the three impact cases treated are listed in table II. (The experimental values also listed in table II are discussed in a subsequent section.)

Figure 2 presents time-history comparisons of solutions of the free-trim equations with fixed-trim solutions for the three cases of theoretical initial conditions given in table II. The quantities plotted are the vertical and angular displacements, velocities, and accelerations.

The free-trim solutions were obtained by the method described in appendix A and the fixed-trim solutions were obtained by the method of reference 7. The so-called $\ddot{\tau}$ curves for fixed trim shown in the plots were obtained by using equation (3) but with the fixed-trim total moment from equation (B7) instead of the free-trim moment. These $\ddot{\tau}$ curves can be interpreted as a measure of the applied moment since, from equation (3), $\ddot{\tau} = \frac{M_{cg}}{I_{cg}}$ and I_{cg} is the constant value for the free-trim float.

EXPERIMENTAL RESULTS

To demonstrate the effects of freedom in trim experimentally, both free- and fixed-trim tests of a float model were made in the Langley impact basin. The measured motions are compared in this section.

No direct comparison between the experimental and theoretical results can be made because of differences between the float used in the tests and that assumed in the theory. The float used in the tests had a pointed step, flared chines, and an afterbody; whereas the theory applies to a float forebody having a transverse step and an infinitely wide V-bottom. Since these float tests represent the only free-trim impact-basin data now available, however, the results are included herein for the qualitative comparisons that can be made.

Apparatus and instrumentation.- The Langley impact basin and testing procedure are described in reference 8. Pertinent dimensions of the float model used in the experiments are given in table I. This model, except for the differences outlined previously, is a $\frac{1}{2}$-scale model of the float considered in the theoretical solutions.

In the free-trim tests the float model was attached to the dropping linkage of the launching carriage at two main pivot points; these supports were on a transverse line which passed through the point corresponding to the center of gravity of the airplane from which the float was patterned. For the fixed-trim tests a third support point was located about 20 inches aft of the main supports on the longitudinal center line of the float.

For the free-trim tests the model was supported only at the two main points and was held at fixed trim until just prior to contact by means of a locking mechanism. After contact the model was free to rotate in pitch about the main supports over a trim range of -6.5° to 22.5°. Beyond those limits angular displacement of the float was restrained by two shock struts which were coupled to the float by means of telescoping tubes, one 60 inches forward and one 60 inches aft of the main pivots. The buffer action of the shock struts extended the trim range about 5° in each direction before a stop was reached.

Two strain-gage accelerometers of the same type of construction were electrically connected to obtain angular acceleration directly. These accelerometers were located on a longitudinal line passing through the axis of rotation and at a distance of 6 feet forward and 6 feet aft of this axis. A control-position transmitter was adapted to the equipment to measure angular displacement.

A standard NACA three-component accelerometer was used to obtain the vertical component of acceleration of the float. It had a natural frequency of 21 cycles per second and a critical damping of 0.8. Otherwise, the standard instrumentation as described in reference 8 was used.

Comparison of free- and fixed-trim experimental results.- Figure 3 presents the comparison of free-trim and fixed-trim experimental results

for cases I and II listed in table II. Again vertical and angular displacements, velocities, and accelerations are compared; the values shown apply to full-scale conditions.

It can be noted in table II that the initial vertical velocity of the fixed-trim run of case I was higher than that of the corresponding free-trim run. The time histories for the fixed-trim run were therefore adjusted as follows to give more comparable results in figure 3(a). Since the initial flight-path angles of the two runs were not greatly different and the initial trims were the same, the velocity time history of the fixed-trim run was scaled by the ratio of the free-trim initial velocity to the fixed-trim initial velocity, the acceleration time history was scaled by the square of this ratio, and the time was scaled by the reciprocal of the ratio. No corresponding adjustments were made for case II.

DISCUSSION

Initial conditions.- Table II presents the initial conditions for both the free- and fixed-trim theoretical solutions and also for the free- and fixed-trim test runs. The test runs were made with a $\frac{1}{2}$-scale model but the initial conditions are given in terms of full-scale values.

The initial conditions for the theoretical solutions of cases I and II were chosen to correspond to the free-trim experimental runs of those cases to make the results as comparable as possible. The experimental fixed-trim runs were chosen, from among those available, to correspond as closely as possible to the respective free-trim runs.

The initial conditions for case III represent a more severe impact such as might occur in a second or third contact during a landing run or in a contact against the flank of an advancing wave.

Case I.- The first set of conditions treated (case I) represents an impact at moderate initial values of flight-path angle and trim. In both the theoretical (fig. 2(a)) and the experimental (fig. 3(a)) results, the vertical motions, trim, and angular velocity for the free-trim condition differ only slightly from the corresponding motions in the fixed-trim condition. The only angular acceleration or moment of any size is exhibited by the experimental free-trim run ($t \approx 0.15$), but this moment is associated with the immersion of the flared chines. Thus, for the initial conditions of case I no significant difference appears to exist between fixed- and free-trim impacts.

Case II.- Case II has approximately the same initial flight-path angle as case I but has a higher initial trim. The vertical motions for the free-trim condition are again observed to approximate those for the fixed-trim condition in both the theoretical (fig. 2(b)) and experimental (fig. 3(b)) curves. This impact, however, resulted in an appreciable change of attitude and a moderate nose-down moment.

The initial trends of the theoretical and experimental angular motions are similar. However, the immersion of the flared chines probably caused large loads on the float forward of the center of rotation and therefore a large nose-up moment as indicated by the positive peak of the experimental $\ddot{\tau}$ curve. These loads would result in large deviations of the subsequent motions of the test float from those of the float assumed in the theory.

Case III.- Case III represents a high-flight-path-angle, low-trim condition such as might occur in an impact on the flank of a wave. The curves represent the "effective" values referred to the inclined plane of the water surface as in reference 9 and are analyzed as an extreme condition of smooth-water impact.

In this case, the deviations between the fixed-trim and free-trim results are much greater than those previously described; freedom in trim in fact reduces appreciably the maximum values of $\ddot{y}$ and $\ddot{\tau}$. The large values of negative vertical velocity of the free-trim solution compared with the fixed-trim solution late in the impact appear to be consistent with the large values of trim attained.

Probably the most serious effect observed for the free-trim solution is the high trim and large positive value of angular velocity at the end of the impact. This could result in a stalled condition between impacts or could lead to extreme initial conditions for a subsequent impact. However, these conditions should be somewhat restricted by the presence of an afterbody and by aerodynamic moments not taken into account by the present theory.

No impact-basin data have been obtained for conditions as severe as those in this case. An indication of the motions to be expected, however, can be obtained from an impact of a four-engine flying boat, the data for which have not been published. The initial conditions for this impact were substantially the same as those of case III and the resulting motions were also very similar. Of particular interest in this seaplane impact is the increase in trim from a small initial value (about 3°) to about 15° with positive angular velocity at the time of exit from the water. The acceleration records contained large oscillations, due probably to structural vibrations, which rendered them unsuitable for direct comparison with the theory; however, the peak values of the faired curves for both $\ddot{y}$ and $\ddot{\tau}$ agree roughly with the

corresponding values for the free-trim solution of case III. Thus, although direct comparison is not practicable, this flying-boat impact indicates that the initial conditions for case III are within the practical range and that the theoretical results which are obtained for this case are at least consistent with flight experience.

General discussion.- In general, for cases I and II, the theoretical free-trim vertical motions approximate the fixed-trim vertical motions to about the same degree as was found experimentally. Also, the trends of the theoretical angular motions are similar to those of the experimental data except where deviation is to be expected because of differences in body shape. Thus, for impacts having moderate initial conditions the theoretical and experimental free-trim results appear to be in agreement.

For the more extreme initial conditions of case III, there is, of course, more deviation of all variables from the fixed-trim solution. The deviations which occur are, however, consistent among themselves and with general experience. Also, the reductions of maximum applied load and moment which occur are to be expected.

CONCLUDING REMARKS

Equations of motion are derived and presented for free-trim hydrodynamic impact of a V-bottom, transverse step, prismatic float forebody. The equations are an extension of previously published fixed-trim hydrodynamic impact theory and are chiefly based on the same concepts and assumptions. A method of solution of the equations is also presented which gives the results as time histories of vertical, horizontal, and angular displacement, velocity, and acceleration.

The free-trim equations are shown to be reducible to the fixed-trim case. Moreover, comparisons of specific solutions of the free-trim equations with fixed-trim solutions for the same initial conditions and also with some experimental data have shown that the computed results are reasonable. The free-trim solutions and experimental data exhibit similar trends and deviations from the fixed-trim case, and changes of attitude and applied moment are consistent with previous experience.

Although these facts do not completely validate the equations, they at least indicate that reasonable and consistent results can be

obtained by their use. Further experimental investigation should provide a better evaluation of the method.

Langley Aeronautical Laboratory
National Advisory Committee for Aeronautics
Langley Field, Va., February 13, 1952

APPENDIX A

METHOD OF SOLUTION

Before the numerical solution can be performed, equations (17) and (20) must be transformed into forms better suited to the method of solution used. Equation (7) is already in the form required for solution.

Equation (17) can be rewritten as

$$\ddot{A\tau} + \ddot{By} = C \tag{A1}$$

and equation (20) as

$$\ddot{D\tau} + \ddot{Ey} = F \tag{A2}$$

where

$$A = \frac{K\varphi(A)\left[y^4(4 \sin^3\tau \cos \tau - \sin \tau \cos \tau) + y^3(4b \sin^3\tau \cos^2\tau)\right]}{12 \sin^3\tau \cos^5\tau} +$$

$$m_f\left(\frac{b \sin \tau}{\cos \tau} - a\right) \tag{A3}$$

$$B = \frac{K\varphi(A)\left[y^3(4 \sin^2\tau \cos^2\tau)\right]}{12 \sin^3\tau \cos^5\tau} + \frac{m_f}{\cos \tau} \tag{A4}$$

$$C = -\frac{K\varphi(A)}{12 \sin^3\tau \cos^5\tau}\left\{y^4\left[\dot{\tau}^2(16 \sin^4\tau - 6 \sin^2\tau + 2)\right] + y^3\left[\dot{\tau}^2(4a \sin^3\tau \cos^2\tau) + \ddot{x}\tau(20 \sin^4\tau \cos^2\tau) + \ddot{y}\tau(12 \sin\tau \cos^3\tau - 20 \sin\tau \cos^5\tau)\right] + y^2\left[12 \sin^2\tau \cos^4\tau(\dot{y} \cos\tau + \dot{x} \sin\tau)^2\right]\right\} - m_f\left(\frac{a\dot{\tau}^2 \sin\tau}{\cos\tau} + b\dot{\tau}^2\right) \quad (A5)$$

$$D = \frac{K\varphi(A)}{60 \sin^4\tau \cos^5\tau}\left[y^5(5 \sin^3\tau \cos\tau - 2 \sin\tau \cos\tau) + y^4(5a \sin^2\tau \cos\tau - 20a \sin^4\tau \cos\tau + 5b \sin^3\tau \cos^2\tau) - y^3(20ab \sin^4\tau \cos^2\tau)\right] - I_{cg} \quad (A6)$$

$$E = \frac{K\varphi(A)}{60 \sin^4\tau \cos^5\tau}\left[y^4(5 \sin^2\tau \cos^2\tau) - y^3(20a \sin^3\tau \cos^2\tau)\right] \quad (A7)$$

$$F = -\frac{K\varphi(A)}{60 \sin^4\tau \cos^5\tau}\left\{y^5\left[\dot{\tau}^2(25 \sin^4\tau - 19 \sin^2\tau + 6)\right] + \right.$$

$$y^4\left[\dot{\tau}^2(35a \sin^3\tau - 85a \sin^5\tau - 10a \sin\tau) + \ddot{x}\dot{\tau}(25 \sin^2\tau \cos^2\tau - \right.$$

$$35 \sin^2\tau \cos^4\tau) + \ddot{y}\dot{\tau}(15 \sin\tau \cos^3\tau - 35 \sin\tau \cos^5\tau)\left.\right] -$$

$$y^3\left[\dot{\tau}^2(20a^2 \sin^4\tau \cos^2\tau) + \ddot{x}\dot{\tau}(100a \sin^5\tau \cos^2\tau) - \ddot{y}\dot{\tau}(40a \sin^2\tau \cos^3\tau - \right.$$

$$100a \sin^4\tau \cos^3\tau) - 20 \sin^2\tau \cos^4\tau(\dot{y} \cos\tau + \dot{x} \sin\tau)^2\left.\right] -$$

$$\left. y^2\left[60a \sin^3\tau \cos^4\tau(\dot{y} \cos\tau + \dot{x} \sin\tau)^2\right]\right\} \tag{A8}$$

Equations (A1) and (A2) can be solved simultaneously to give

$$\ddot{y} = \frac{AF - DC}{AE - DB} \tag{A9}$$

and

$$\ddot{\tau} = \frac{EC - BF}{EA - BD} \tag{A10}$$

which, together with equation (7),

$$\ddot{x} = \frac{\ddot{y} \sin\tau}{\cos\tau} + \frac{a\dot{\tau}^2}{\cos\tau} + \frac{b\ddot{\tau}}{\cos\tau}$$

are the equations to be used in the numerical solution.

The numerical solution can be performed by extrapolation of the plots of $\ddot{y}$ and $\ddot{\tau}$ against time by any desired function to obtain an approximate value at the end of the next time interval. The other quantities ($\ddot{x}$, $\dot{x}$, x, $\dot{y}$, y, $\dot{\tau}$, and τ) are then computed and the process iterated. By this method, time-history plots of each of the nine variables are obtained. The present solutions were made, however, by the Kutta $\frac{3}{8}$ method (reference 10) which is more readily adaptable to the automatic computing machine used.

APPENDIX B

REDUCTION TO FIXED-TRIM CASE

One test of the validity of the free-trim equations is their compatibility with the special, and well-established, case of fixed-trim impact. If, in equation (17), the trim is considered to remain constant throughout the impact, all terms containing derivatives of the trim are eliminated and the equation becomes

$$\frac{K\varphi(A)}{12 \sin^3\tau \cos^5\tau}\left[4y^3\ddot{y}\dot{\tau} \sin^2\tau \cos^2\tau + 12y^2\dot{\tau}\sin^2\tau \cos^4\tau(\dot{y} \cos \tau + \dot{x} \sin \tau)^2\right] =$$

$$-m_f \frac{\ddot{y}}{\cos \tau} \tag{B1}$$

which reduces to

$$-\frac{m_f\ddot{y}}{\cos \tau} = \frac{K\varphi(A)y^3\ddot{y}\dot{\tau}}{3 \sin \tau \cos^3\tau} + \frac{K\varphi(A)y^2(\dot{y} \cos \tau + \dot{x} \sin \tau)^2}{\sin \tau \cos \tau} \tag{B2}$$

However,

$$\frac{\ddot{y}}{\cos \tau} = \ddot{z} = \frac{dV_n}{dt} \tag{B3}$$

and

$$V_n = \dot{y} \cos \tau + \dot{x} \sin \tau \tag{B4}$$

so that, by introducing equations (2), (B3), and (B4) into equation (B2),

$$F_n = \frac{K\varphi(A)y^3 \frac{dV_n}{dt}}{3 \sin \tau \cos^2\tau} + \frac{K\varphi(A)y^2{V_n}^2}{\sin \tau \cos \tau} \tag{B5}$$

which corresponds to equation (22) of reference 1.

Similarly, the right-hand side of equation (20) is equal to the moment about the center of gravity as in equation (3) and, if the trim derivatives are set equal to zero in the left-hand side, the equation becomes

$$\frac{K\varphi(A)}{60 \sin^4\tau \cos^5\tau}\left[5y^4\ddot{y} \sin^2\tau \cos^2\tau - 20ay^3\ddot{y} \sin^3\tau \cos^2\tau + \right.$$

$$20y^3\sin^2\tau \cos^4\tau(\dot{y} \cos \tau + \dot{x} \sin \tau)^2 -$$

$$\left. 60ay^2\sin^3\tau \cos^4\tau(\dot{y} \cos \tau + \dot{x} \sin \tau)^2\right] = M_{cg} \tag{B6}$$

which reduces to

$$M_{cg} = \frac{K\varphi(A)y^4\ddot{y}}{12 \sin^2\tau \cos^3\tau} + \frac{K\varphi(A)y^3(\dot{y} \cos \tau + \dot{x} \sin \tau)^2}{3 \sin^2\tau \cos \tau} - \frac{K\varphi(A)ay^3\dot{y}}{3 \sin \tau \cos^3\tau} -$$

$$\frac{K\varphi(A)ay^2(\dot{y} \cos \tau + \dot{x} \sin \tau)^2}{\sin \tau \cos \tau} \tag{B7}$$

After equations (B3) and (B4) are substituted into equation (B7), the moment becomes

$$M_{cg} = \frac{K\varphi(A)}{3 \sin^2\tau \cos^3\tau}\left[\frac{y^4\ddot{y}}{4} + y^3\cos^2\tau(\dot{y} \cos \tau + \dot{x} \sin \tau)^2\right] -$$

$$a\left[\frac{K\varphi(A)y^3 \frac{dV_n}{dt}}{3 \sin \tau \cos^2\tau} + \frac{K\varphi(A)y^2V_n^2}{\sin \tau \cos \tau}\right] \tag{B8}$$

and, by introducing equation (B5) and equations (9) and (11) of reference 3, equation (B8) becomes

$$M_{cg} + aF_n = \frac{K\varphi(A)}{3 \sin^2\tau \cos^3\tau}\left[\frac{y^4\ddot{y}}{4} + y^3(\dot{y} + K_1 \cos \tau)^2\right] \tag{B9}$$

where K_1 is K in reference 3.

From equations (34) and (26) of reference 6 the moment about the step is

$$M_s = M_{cg} + aF_n \tag{B10}$$

Substituting equation (B10) into equation (B9) gives the moment about the step

$$M_s = \frac{K\varphi(A)}{3 \sin^2\tau \cos^3\tau}\left[\frac{y^4\ddot{y}}{4} + y^3(\dot{y} + K_1 \cos \tau)^2\right] \tag{B11}$$

which is identical with equation (16) of reference 6.

Equation (7) can also be reduced in this manner to give

$$\ddot{x} = \ddot{y} \tan \tau \tag{B12}$$

In the fixed-trim condition the step motions and center-of-gravity motions are the same. Equation (B12) is, therefore, equivalent to

$$\ddot{X} = \ddot{Y} \tan \tau \tag{B13}$$

Equation (B13) can readily be deduced from figure 1(c).

REFERENCES

1. Mayo, Wilbur L.: Analysis and Modification of Theory for Impact of Seaplanes on Water. NACA Rep. 810, 1945. (Supersedes NACA TN 1008.)

2. Benscoter, Stanley U.: Impact Theory for Seaplane Landings. NACA TN 1437, 1947.

3. Milwitzky, Benjamin: A Generalized Theoretical and Experimental Investigation of the Motions and Hydrodynamic Loads Experienced by V-Bottom Seaplanes during Step-Landing Impacts. NACA TN 1516, 1948.

4. Wagner, Herbert: Über Stoss- und Gleitvorgänge an der Oberfläche von Flüssigkeiten. Z.f.a.M.M., Bd. 12, Heft 4, Aug. 1932, pp. 193-215.

5. Pabst, Wilhelm: Theory of the Landing Impact of Seaplanes. NACA TM 580, 1930.

6. Milwitzky, Benjamin: A Generalized Theoretical Investigation of the Hydrodynamic Pitching Moments Experienced by V-Bottom Seaplanes during Step-Landing Impacts and Comparisons with Experiment. NACA TN 1630, 1948.

7. Mayo, Wilbur L.: Theoretical and Experimental Dynamic Loads for a Prismatic Float Having an Angle of Dead Rise of $22\frac{1}{2}^{\circ}$. NACA RB L5F15, 1945.

8. Batterson, Sidney A.: The NACA Impact Basin and Water Landing Tests of a Float Model at Various Velocities and Weights. NACA Rep. 795, 1944. (Supersedes NACA ACR L4H15.)

9. Miller, Robert W.: Hydrodynamic Impact Loads in Rough Water for a Prismatic Float Having an Angle of Dead Rise of 30°. NACA TN 1776, 1948.

10. Levy, H., and Baggott, E. A.: Numerical Studies in Differential Equations. Vol. I, Watts & Co. (London), 1934, p. 104.

TABLE I

PHYSICAL CHARACTERISTICS OF FULL-SCALE HULL AND $\frac{1}{2}$ - SCALE EXPERIMENTAL MODEL

	Full-scale hull	Experimental model ($\frac{1}{2}$ - scale)
Beam, ft	6.33	3.17
Forebody length, from centroid of step, ft	19.11	9.56
Over-all length, ft	35.67	17.83
a (from centroid of step), ft	2.28	1.14
b (normal to keel), ft	6.06	3.03
Weight, lb	14,000	1,750
m_f, lb-sec^2/ft	434.78	54.35
I_{cg}, lb-sec^2-ft	19,410	607
β, deg	20	20

TABLE II

INITIAL CONDITIONS FOR TIME HISTORIES

	Case I			Case II			Case III
	Theoretical free and fixed trim	Experimental (a)		Theoretical free and fixed trim	Experimental (a)		Theoretical free and fixed trim
		Free trim	Fixed trim		Free trim	Fixed trim	
y_o, ft	0	0	0	0	0	0	0
$\dot{y}_o$, ft/sec	11.5	11.5	13.9	10.8	10.8	9.5	19.1
$\ddot{y}_o$, ft/sec/sec	0	0	0	-5.8	-5.8	0	0
x_o, ft	0	0	0	0	0	0	0
$\dot{x}_o$, ft/sec	120.4	120.4	125.7	123.7	123.7	125.7	90.0
$\ddot{x}_o$, ft/sec/sec	0	0	0	0	0	0	0
τ_o, radians	0.122	0.122	0.122	0.201	0.209	0.209	0.052
τ_o, deg	7.0	7.0	7.0	11.5	12.0	12.0	3.0
$\dot{\tau}_o$, radians/sec	0	0	-------	0	0	-------	0
$\ddot{\tau}_o$, radians/sec/sec	0	0	-------	0	0	-------	0
γ_o, deg	5.4	5.4	6.2	5.0	5.0	4.4	12.0

[a]Experimental values changed to full-scale.

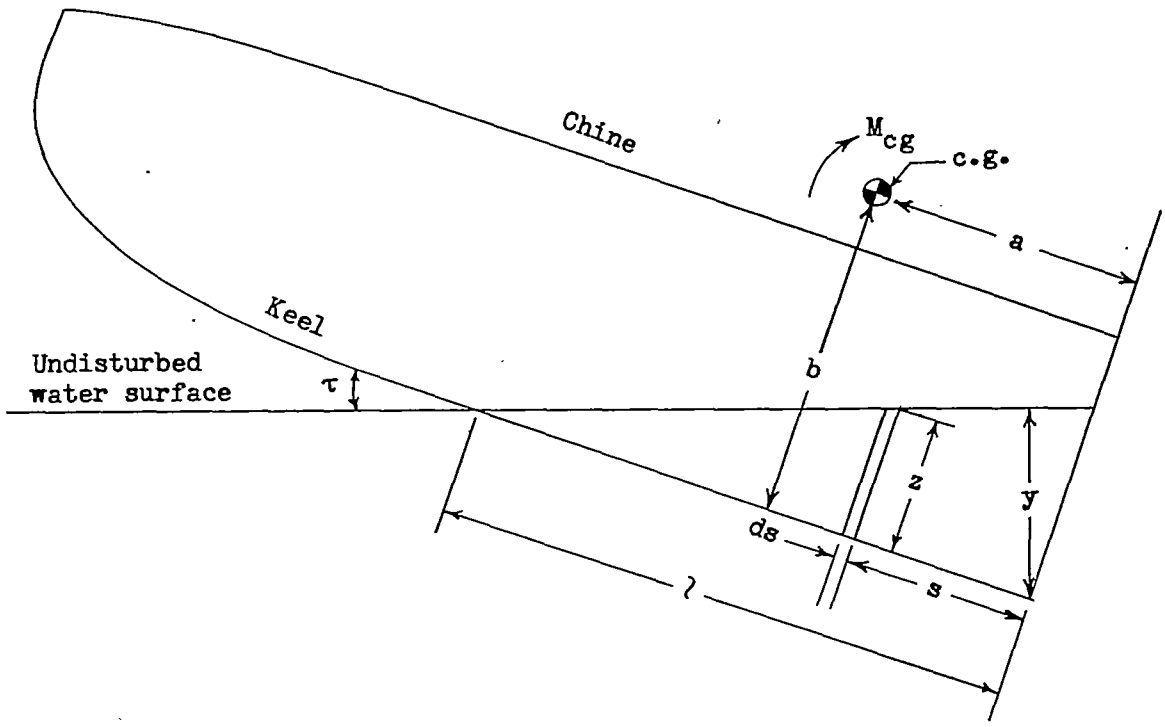

(a) Sketch of float during impact.

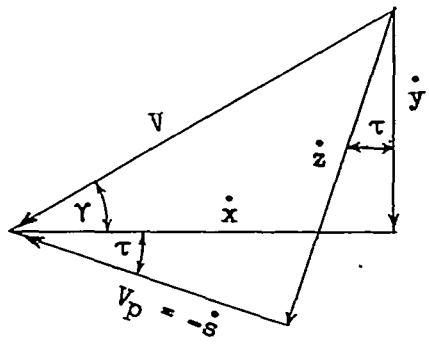

(b) Velocity components.

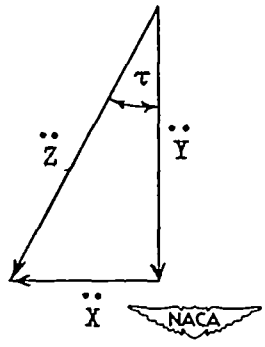

(c) Components of center-of-gravity acceleration.

Figure 1.- Schematic representation of impact.

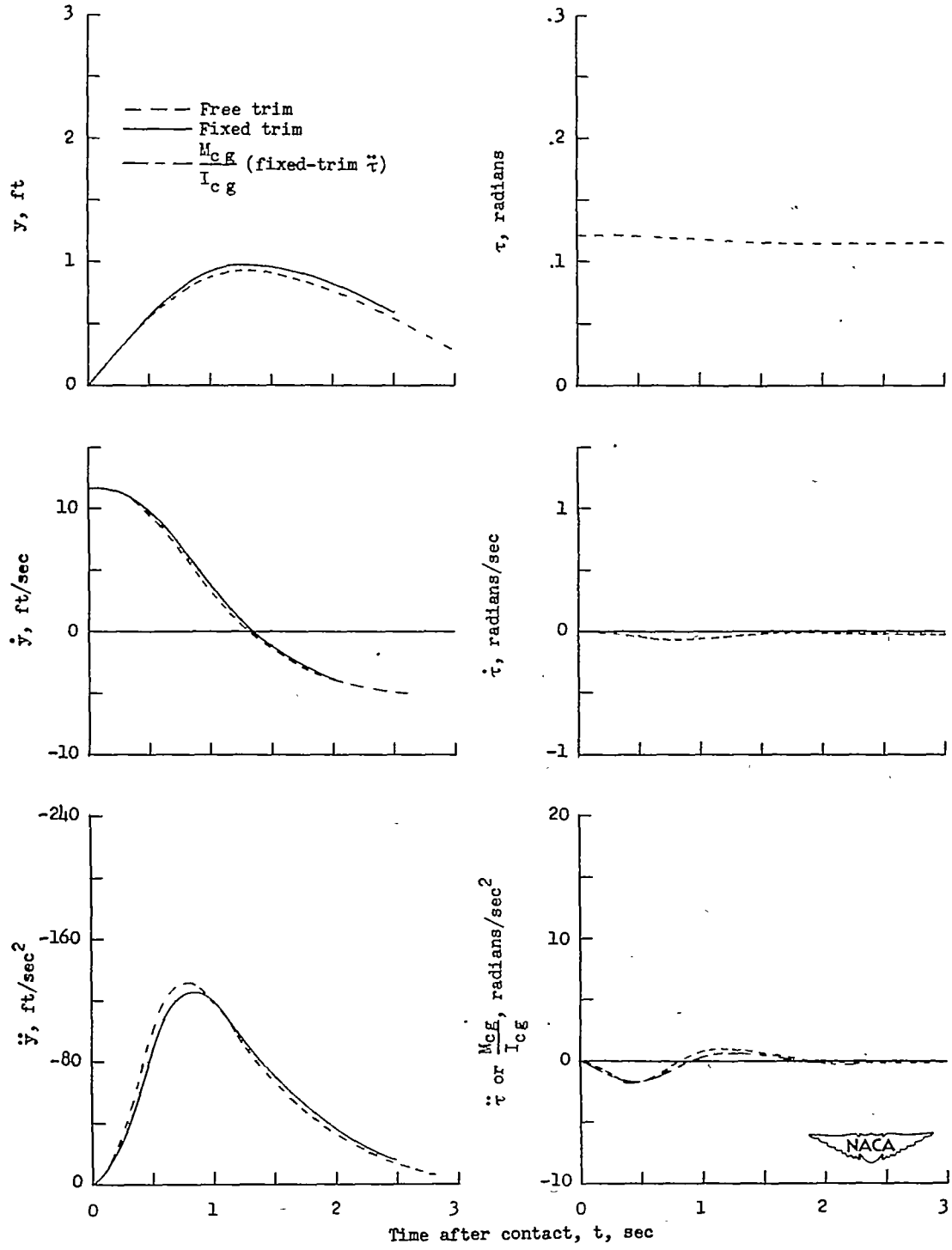

(a) Case I; $\tau_o = 7.0^\circ$ or 0.122 radian; $\gamma_o = 5.4^\circ$.

Figure 2.- Comparison of theoretical free-trim and fixed-trim float motions.

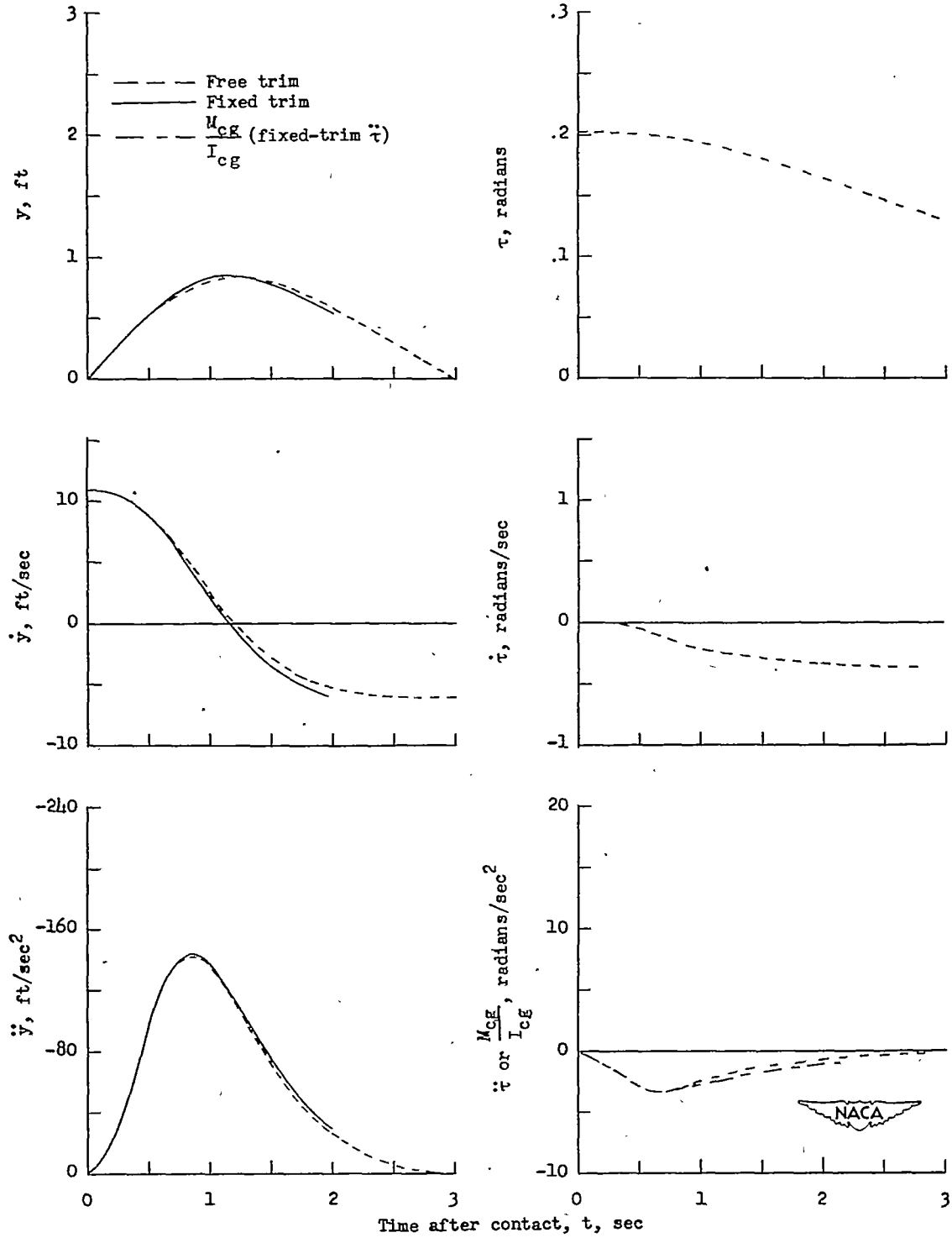

(b) Case II; τ_o = 11.5° or 0.201 radian; γ_o = 5.0°.

Figure 2.- Continued.

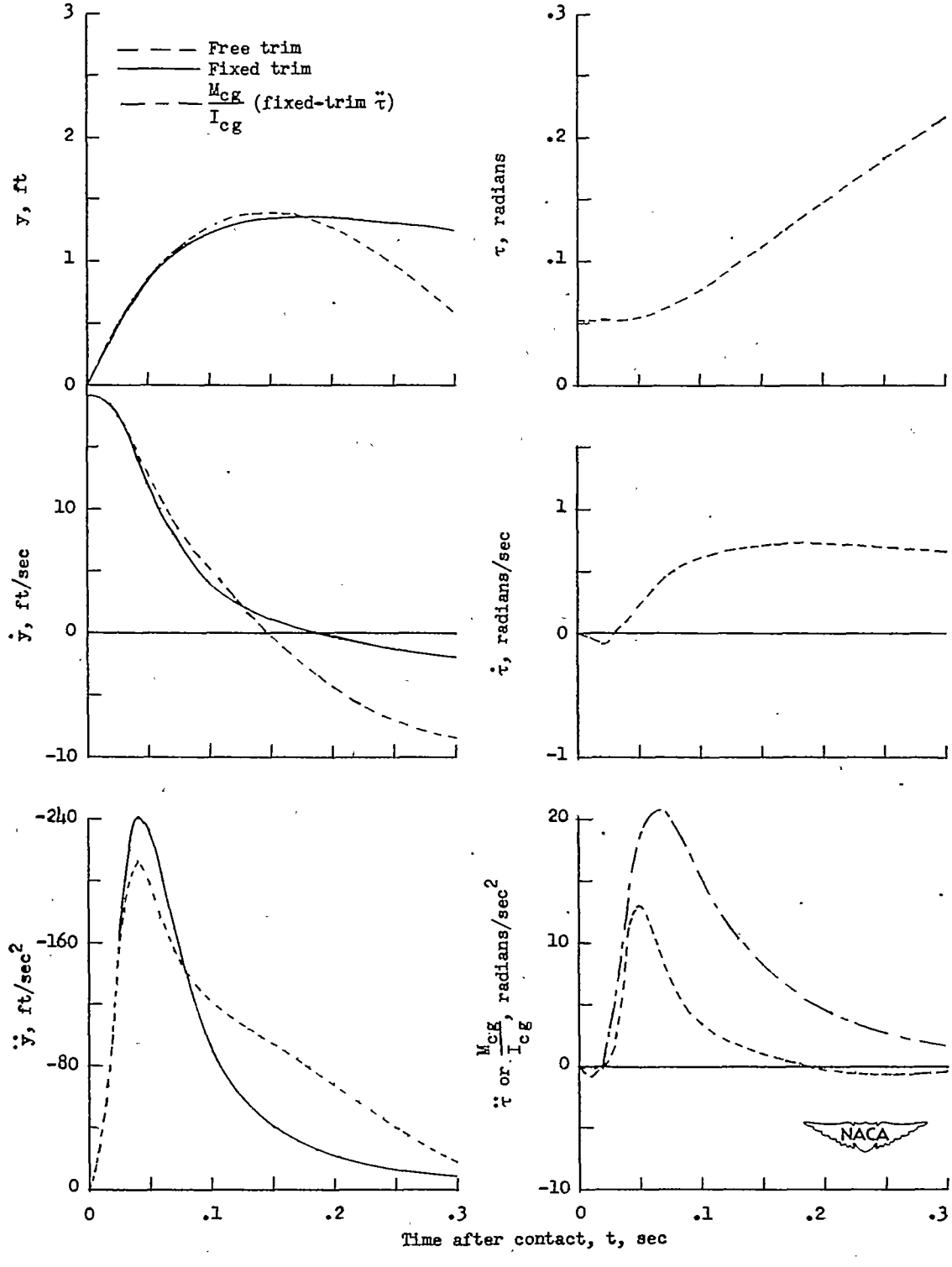

(c) Case III; τ_o = 3.0° or 0.052 radian; γ_o = 12.0°.

Figure 2.- Concluded.

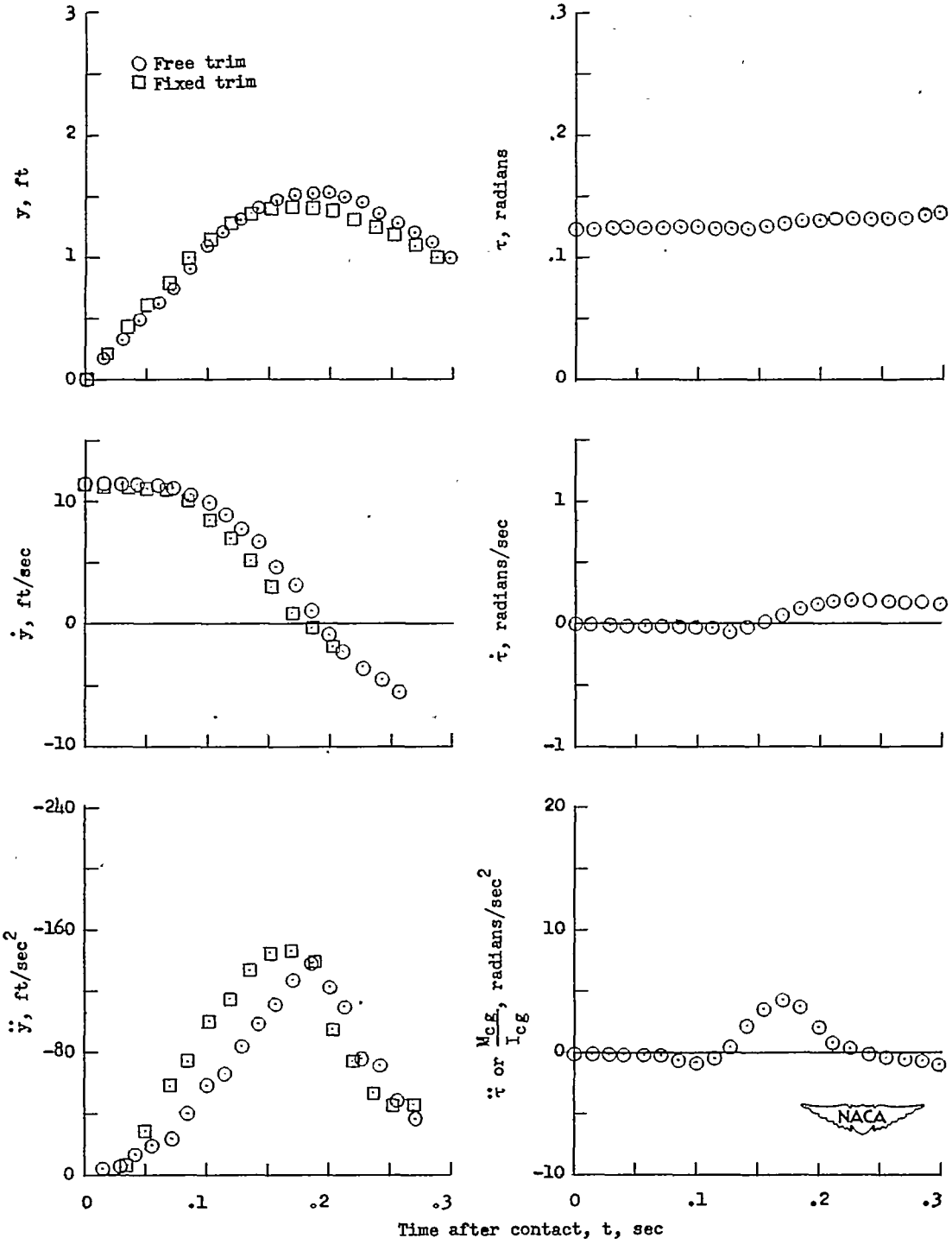

(a) Case I; $\tau_o = 7.0^\circ$ or 0.122 radian; $\gamma_o = 5.4^\circ$.

Figure 3.- Comparison of experimental free-trim and fixed-trim float motions.

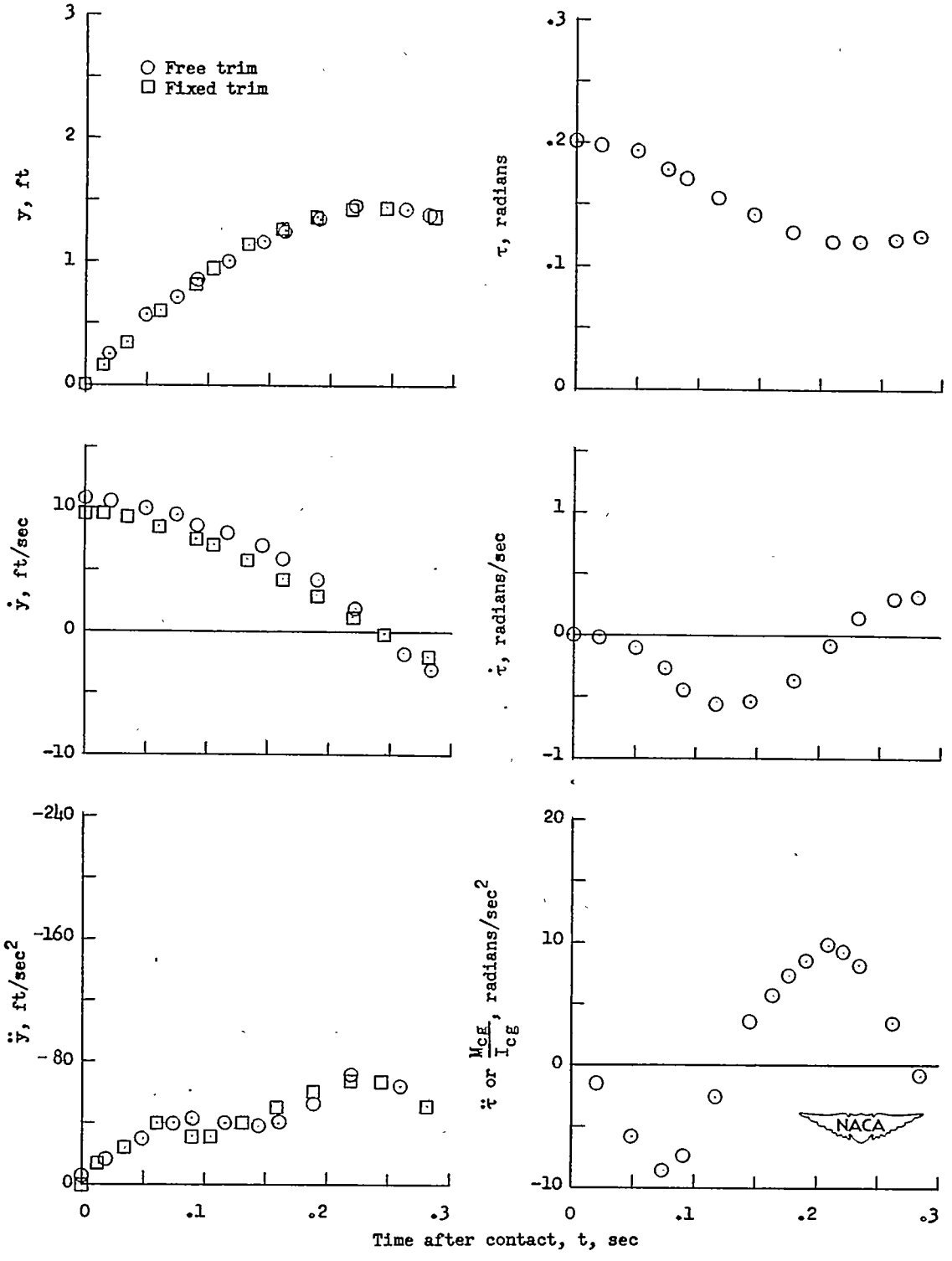

(b) Case II; $\tau_o = 12.0^\circ$ or 0.209 radian; $\gamma_o = 5.0^\circ$.

Figure 3.- Concluded.

NACA-Langley - 8-25-52 - 1000